

Title No. 114-S120

# Response of Heavily Reinforced High-Strength Concrete Coupling Beams

by Andrew W. Fisher, Evan C. Bentz, and Michael P. Collins

*Understanding the strength and stiffness of coupling beams is essential when determining the lateral performance of coupled shear wall high-rise concrete buildings. This paper investigates these properties using full-scale experiments and comparative analytical studies. Adequate strength and ductility can be achieved with shear-critical coupling beams by using large amounts of well-detailed stirrups, even if these exceed the ACI Code upper limits on shear capacity. These limits are shown to penalize the strength of heavily reinforced, high-strength concrete coupling beams. Shear and localized wall deformations contribute significantly to the overall beam response. Ignoring either of these deformations can result in over-predicting the lateral stiffness of the building. The new program Response is shown to be a powerful tool to accurately predict load-deformation behavior, having an average test-to-prediction ratio for shear strength of 1.04, and 1.14 for the displacement at peak load.*

**Keywords:** coupling beams; cover spalling; maximum shear strength; shear strain; stiffness; strain penetration.

## INTRODUCTION

Coupling beams in coupled shear wall high-rise buildings experience significant shear and flexural demand in high wind or earthquake events, as shown in Fig. 1(a). The depth of these beams may control the story-to-story height, shown in Fig. 1(b), hence playing an important role in the cost effectiveness of the structure. These conditions often result in coupling beam designs that are compact, use large amounts of reinforcement, and are heavily loaded in shear. Experiments<sup>1–9</sup> have shown that adequate strength and ductility can be achieved with coupling beams designed to fail in flexure; however, few tests involve coupling beams designed to fail in shear by yielding of the stirrups prior to the longitudinal reinforcement. The limits on shear capacity imposed by the ACI Code<sup>10</sup> prevent large amounts of stirrups from being used in coupling beams to obtain high design shear strengths. This paper will demonstrate that high strength and ductility can be achieved with coupling beams designed to fail in shear by using well detailed stirrups that exceed the ACI Code limits.

When modeling a high-rise concrete building, the stiffness assigned to a coupling beam plays a critical role in predicting the lateral behavior of the structure. This paper will show that an accurate coupling beam stiffness model must take into account both flexural and shear deformations. The shear deformations can be equal to or even greater than the flexural deformations based on the span-depth ratio.<sup>11</sup> Localized deformations and a reduced stiffness at the beam-wall joints due to reinforcement slip and extension<sup>11–13</sup> are also shown to influence the coupling beam stiffness. These

stiffness calculations will demonstrate that high ductility can be achieved with shear critical members prior to yielding of the longitudinal reinforcement.

This paper will describe an experimental investigation of four heavily reinforced, high-strength concrete coupling beam specimens that were loaded to failure in shear; refer to Fig. 1(a) and 1(c). The coupling beams had a clear span to overall depth ratio of 2.67, and were hence designed using a conventional reinforcement layout.<sup>4</sup> The primary variables altered between the specimens were the side cover thickness, concrete compressive strength, and shear reinforcement ratio. Three of the four specimens exceeded the upper shear limits imposed by the ACI Code. The observed behavior of the coupling beam specimens will be compared to the shear strength predictions of the ACI and CSA<sup>14</sup> design codes, as well as to the predictions made by programs Membrane<sup>15</sup> and Response.<sup>16</sup> Additional observations presented include the strain penetration length of the longitudinal reinforcement into the shear walls, and the influence of load-induced side cover spalling on shear strength.

## RESEARCH SIGNIFICANCE

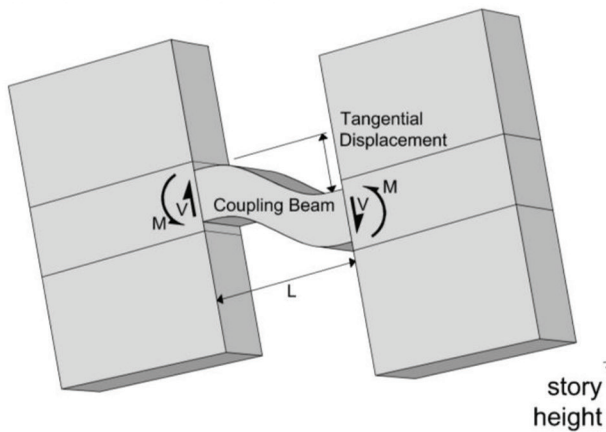
The experiments and analytical studies in this paper will demonstrate that the upper limit on shear capacity imposed by the ACI Code can be liberalized, resulting in more efficient coupling beam design. It is shown that shear and localized wall deformations must be accounted for to obtain accurate estimates of the system stiffness.

## EXPERIMENTAL PROGRAM

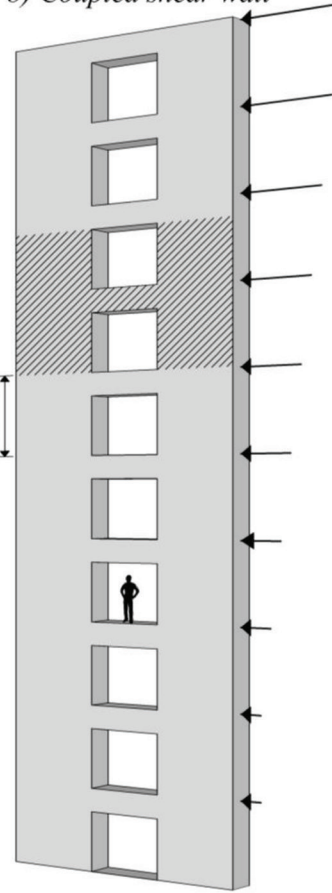
The full set of details for the experimental program are summarized in Fig. 2. To test multiple coupling beams while limiting the amount of construction and materials, a test assembly was developed, shown in Fig. 2(a), to allow an interchangeable coupling beam specimen. This specimen was constructed monolithically with shear wall end blocks. The remaining height of the shear walls were constructed as a set of four components that were reused for each test. The assembly was designed to simulate the double curvature of a coupling beam by applying a point load  $P$  having a line-of-action through the coupling beam centreline. This load was applied through cantilever beams constructed monolithically with two of the shear wall components. High-

*ACI Structural Journal*, V. 114, No. 6, November-December 2017.  
MS No. S-2016-209, doi: 10.14359/51689501, received May 31, 2016, and reviewed under Institute publication policies. Copyright © 2017, American Concrete Institute. All rights reserved, including the making of copies unless permission is obtained from the copyright proprietors. Pertinent discussion including author's closure, if any, will be published ten months from this journal's date if the discussion is received within four months of the paper's print publication.

a) Deformation of coupled shear wall section



b) Coupled shear wall



c) Coupling beam test specimen CBF1

Fig. 1—Coupling beam subjected to shear and bending.

strength post-tensioning bars in cast-in steel ducts were used to post-tension the coupling beam specimen and shear wall components together, creating an average compressive stress of 2 MPa (290 psi) over the horizontal interfaces between the coupling beam and shear wall components.

### Coupling beam specimens

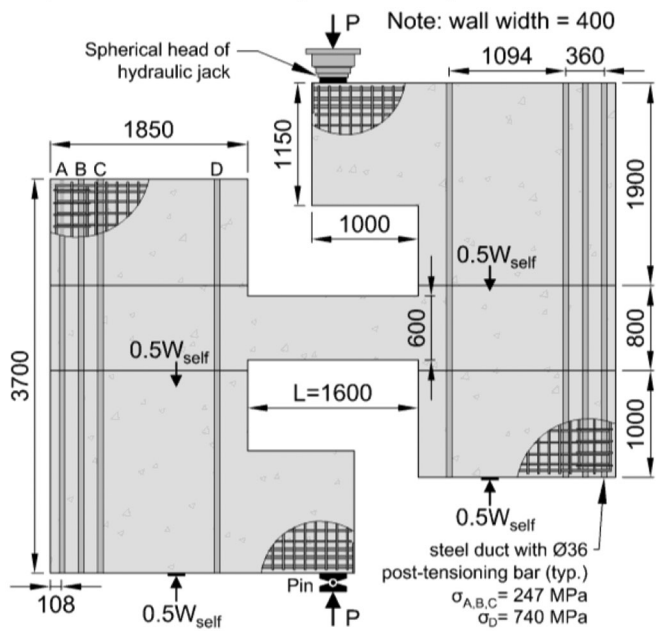
The four coupling beam specimens, named CBF1 to CBF4 in Fig. 2(d), consisted of a 1600 mm (63.0 in.) long and 600 mm (23.6 in.) deep coupling beam constructed monolithically with 400 mm (15.8 in.) wide shear wall end blocks. Specimen CBF1 had a coupling beam width of 316 mm (12.5 in.) with 3 mm (0.1 in.) of side cover. CBF2, CBF3, and CBF4 had a beam width of 400 mm (15.8 in.) with 45 mm (1.8 in.) side cover. All specimens were designed with twelve 30M longitudinal bars near the top and bottom faces of the cross section. The predicted flexural failure load was at least 1.3 times higher than the predicted shear failure load, to ensure that all four specimens would fail in shear. The longitudinal bars continued into the full length of the shear wall end blocks to allow for proper bar development. The transverse reinforcement for the coupling beams was designed using 15M (U.S. No. 5) closed stirrups. Each stirrup wrapped around three of the four rows of longitudinal bars so that the stirrups could be offset along the length of the beam. The stirrups were spaced at 60 mm (1.9 in.) for CBF1, CBF2, and CBF3, resulting in an amount of shear

reinforcement that exceeded the upper limit on shear capacity imposed by the ACI Code. CBF4 had stirrups spaced at 120 mm (4.7 in.), resulting in an amount of shear reinforcement that met the ACI Code. The specimens were cast in pairs using high-strength self-consolidating concrete with a specified maximum aggregate size of 14 mm (0.55 in.). All specimens were moist cured 5 to 7 days and then remained in the climate-controlled laboratory until testing. CBF1 and CBF2 reached a 134-day concrete strength of 80.3 MPa (11.6 ksi), despite having a specified 28-day strength of 50 MPa (7.25 ksi). CBF3 and CBF4 reached a 106-day concrete strength of 66.5 MPa (9.64 ksi), despite having a specified 28-day strength of 30 MPa (4.35 ksi). The measured concrete stiffness  $E_c$  is also presented in Fig. 2(d).

### Boundary conditions

The experimental setup required a single pin support, which had the same line of action as the applied load  $P$ . The loading jack had a spherical head built into it, making it able to act as a pin. The full test assembly weighed approximately 180 kN (40.5 kip). To mitigate the influence of self-weight on the coupling beam behavior, hydraulic jacks were placed under the assembly 1450 mm (57.1 in.) either side of the coupling beam centerline in order to float the self-weight. Each jack supported approximately 90 kN (20.3 kip) during the test, but were able to move as the test assembly deformed.

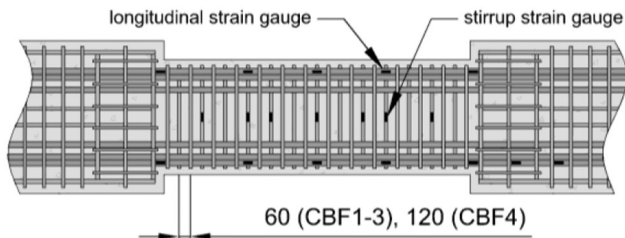
### a) Elevation View of Test Setup



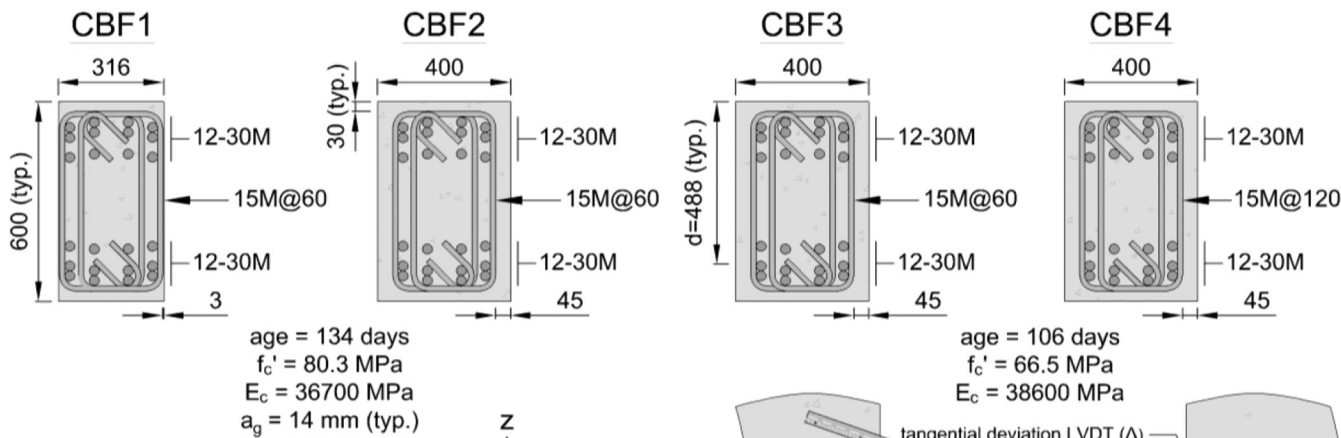
### b) Reinforcement Properties

Bar Size	$A_b$	$f_y$	$\varepsilon_{sh}$	$f_u$	$\varepsilon_u$
	(mm <sup>2</sup> )	(MPa)	(x10 <sup>-3</sup> )	(MPa)	(x10 <sup>-3</sup> )
10M	100	464	10.1	679	123
15M	200	422	22.9	563	163
20M	300	436	16.8	572	153
30M	700	563	16.2	704	101
Ø36-PT	1000	942	-	1126	-

### c) Strain Gauge Layout



### d) Coupling Beam Cross-Sections and Measured Concrete Properties



### e) External Instrumentation

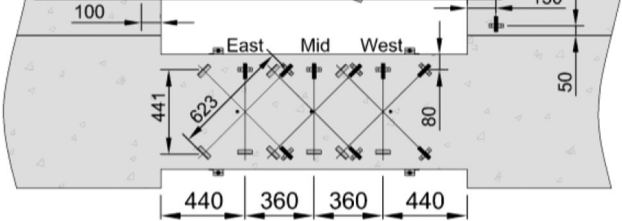
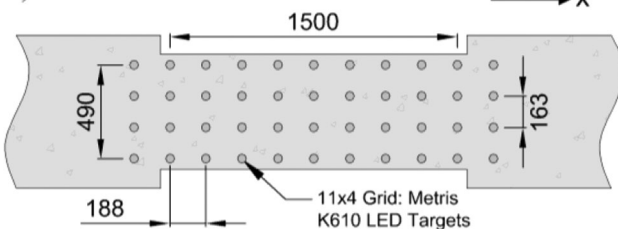


Fig. 2—Reinforcement details, sectional properties, loading, and instrumentation details. (Note: Dimensions in mm; 1 mm = 0.0394 in.; 1 MPa = 145 psi = 0.145 ksi.)

### Instrumentation

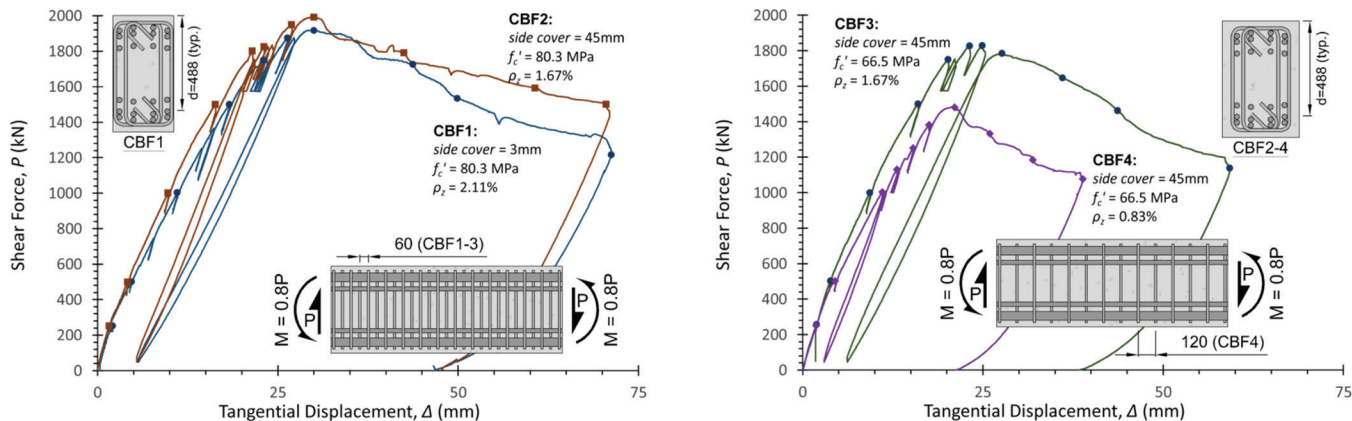
Five strain gauges were installed on each of the top and bottom layers of longitudinal reinforcement; refer to Fig. 2(c). Two additional strain gauges were installed on the longitudinal bars in the east shear wall end blocks. Seven strain gauges were installed middepth on the stirrup legs. These strain gauges alternated on the north and south facing legs of the stirrups to detect any torsion that may have occurred during the test. Nine linearly varying differential trans-

formers (LVDTs) were installed on the north face of the coupling beams, shown in Fig. 2(e). The LVDTs measured the average z-direction (vertical) strain  $\varepsilon_z$  and average shear strain  $\gamma_{xz}$  at midspan and at a distance  $0.9d$  from the shear walls. Instrumentation was also installed on the beam to detect the occurrence of side cover spalling by measuring out-of-plane expansion. The tangential displacement of the coupling beam was obtained by affixing a braced aluminum rod to the east shear wall and recording the vertical displace-

**Table 1—Summary of experimental program**

Specimen	Observations at stirrup yield, $\varepsilon_z = 2.11 \times 10^{-3}$			Observations at peak load					Observations at maximum deformation	
	P, kN	$\Delta$ , mm	v, MPa	P, kN	$\Delta$ , mm	v, MPa	$\varepsilon_{z,max} \times 10^{-3}$	$\gamma_{z,max} \times 10^{-3}$	P, kN	$\Delta$ , mm
CBF1	1696 (East)	22.4	11.00	1918	30.0	12.44	5.66 (East)	7.33 (East)	1217	71.2
CBF2	1755 (West)	22.1	8.991	1992	30.0	10.21	6.70 (East)	5.99 (West)	1503	70.5
CBF3	1700 (West)	20.5	8.709	1830	27.6	9.375	8.95 (West)	4.67 (West)	1138	59.2
CBF4	1308 (East)	16.3	6.701	1481	21.1	7.587	5.43 (East)	4.77 (Mid)	1076	38.8

Notes:  $v = P/b_w d$ ; 1 mm = 0.0394 in.; 1 kN = 0.225 kip; 1 MPa = 145 psi = 0.145 ksi.



Specimen	Applied Load P, kN						
	LS3	LS4	LS5	LS6	LS7	PEAK	END
CBF1	1002	1501	1751*	1875*	-	1918	1217
CBF2	1002	1501	1801*	1827*	1950	1992	1503
CBF3	1000	1500	1752*	1827*	-	1830*	1138
CBF4	1003*	1130*	1251	1381	-	1481	1076

\*load cycled three times, \*peaked during second cycle

*Fig. 3—Observed load-deflection response with associated load stages. (Note: 1 mm = 0.0394 in.; 1 kN = 0.225 kip.)*

ment of the rod with an LVDT mounted on the west shear wall. Infrared light emitting diode (LED) targets also shown in Fig. 2(e) were installed in a 4 x 11 grid on the south face of the coupling beam to measure local element strains and displacement patterns. Complete details on these experiments are available elsewhere.<sup>17</sup>

### Loading protocol

All of the test specimens were loaded to failure under displacement-controlled monotonic loading. The load was paused at various load stages (LS) to inspect the specimen, take photos, mark crack propagation, and manually measure crack widths. During a load stage, the applied load was reduced by 10% for safety. The load was cycled at the second-to-last and last load stages before the predicted failure load. The machine load was reduced to a value near zero three times, then loaded back up to the load stage value. After reaching the third peak and pausing to inspect the specimen, the load was increased to the next load stage or to failure. Once peak load was reached, the displacement of the loading jack was increased until the applied load was less than 80% of the peak load and the specimen had achieved significant displacements.

## EXPERIMENTAL RESULTS

Table 1 summarizes the results from the experimental program. All specimens failed in shear, which was characterized by yielding of the stirrups followed by slip on the crack, and then diagonal concrete crushing. The full load-displacement response for each specimen is shown in Fig. 3. To better present the data in Fig. 3, only one of the loading cycles is shown for each experiment. All other cycles are truncated at a value 10% below the associated load stage. A summary of load stages is presented at the bottom of Fig. 3. The measurements in Table 1 at stirrup yield correspond to the z-direction (vertical) LVDT that reached the stirrup yield strain of  $2.11 \times 10^{-3}$  first. The location of this LVDT is labeled West, Mid, or East, as shown in Fig. 2(e). The observed peak load strains correspond to the LVDT that measured the highest value. Despite failing in shear, all four specimens exhibited considerable post-peak ductility, in that the reduction in load carrying capacity with increasing deformation was gradual. On average, the deflection was more than doubled yet the specimens were able to maintain about 70% of the peak load.

Strain gauge measurements for specimen CBF1 are shown in Fig. 4. The measured behavior was typical for all four

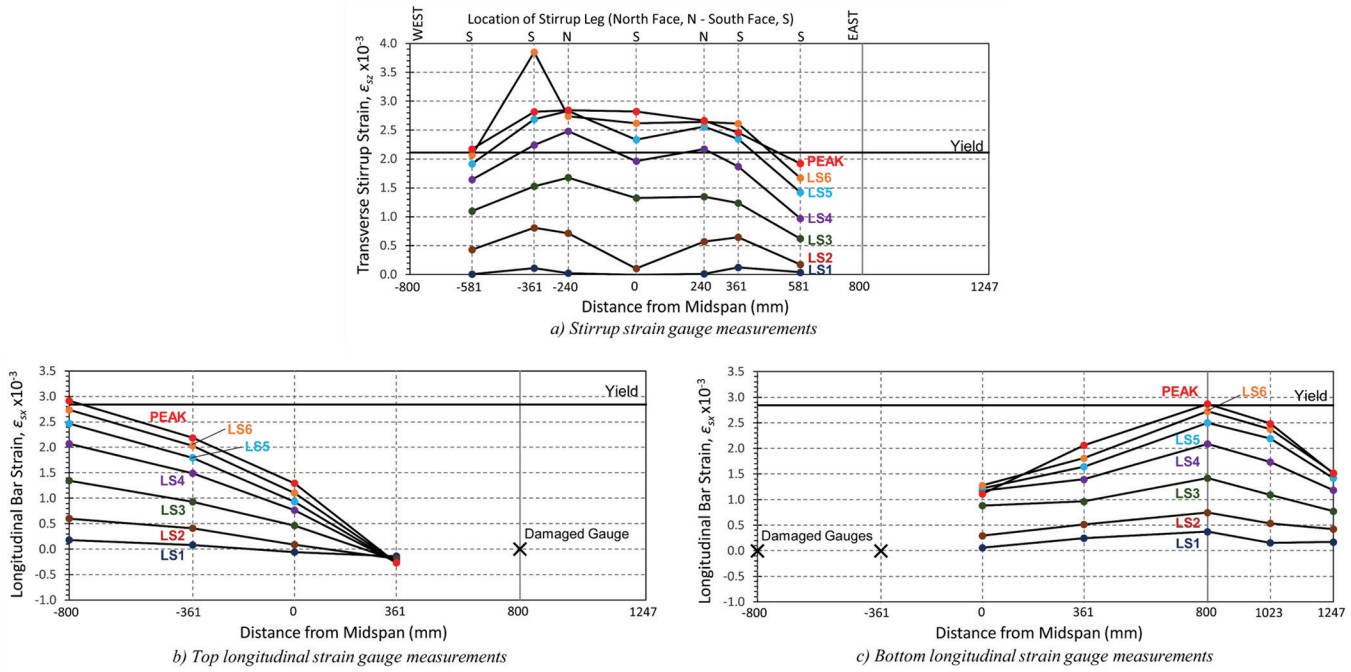


Fig. 4—Longitudinal and transverse reinforcement strains for Specimen CBF1. (Note: 1 mm = 0.0394 in.)

specimens. The critical section for shear was located approximately  $d$  from the face of the shear wall— $\pm 361$  mm ( $\pm 14.2$  in.) from midspan in Fig. 4(a). The stirrup strains measured at the critical sections are higher at LS6 than at the peak load, indicating that a redistribution of stress occurred as these sections began to fail. The stirrup strains between the critical sections are approximately uniform at the peak load. The midspan stirrup strain is approximately zero until LS3 when the first midspan shear cracks formed. The top axis of Fig. 4(a) indicates which stirrup leg the strain gauge was affixed to, indicating a lack of torsional effects. The outer layers of longitudinal reinforcement just began to yield in tension at the peak load; shown in Fig. 4(b) and 4(c). Note that at midspan, where the moment is zero, the strains in both the bottom and top longitudinal reinforcing bars exceed  $1 \times 10^{-3}$ . The location of zero longitudinal strain, where the flexural compression cancels out the tension due to shear, occurred  $\pm 361$  mm ( $\pm 14.2$  in.) from midspan as shown in Fig. 4(b) and 4(c). The highest longitudinal strains occurred at the face of the shear walls, and reduced by almost 50% at a distance of 447 mm (17.6 in.) into the wall. Paulay and Priestley<sup>18</sup> recommend that the yield penetration length  $l_{yp}$  be taken as  $0.022d_b f_y$  mm ( $0.15d_b f_y$  in.) where  $d_b$  is the longitudinal bar diameter and  $f_y$  is the yield strength of the reinforcement, which gives a penetration length of 370 mm (14.6 in.). This significantly underestimates the strain penetration length based on the longitudinal bar strains shown in Fig. 4(c), as well as the observed shear wall crack patterns, shown in Fig. 5 and 6. Based on these crack patterns, the penetration length is estimated to be 1150 mm (45.3 in.), a number that was consistent for all four specimens. This discrepancy could result in an underestimation of coupling beam deflections, and therefore an overestimation of structural stiffness.

Cracks were marked and measured at each load stage. First cracking occurred in the flexural tension region of the

beams. Shear cracks were also observed to form between the flexural compression corners, creating a set of approximately parallel diagonal cracks that covered the full length of the specimens. At the time of failure, the widest shear cracks formed approximately  $d$  away from the face of the shear walls. On average, the maximum crack widths were 2.1 times larger than the average crack widths. Specimen CBF1 was observed to have much smaller crack widths overall than the other three specimens due to a side cover thickness of 3 mm (0.1 in.) versus the 45 mm (1.8 in.) for the other three specimens. The further away the concrete surface is from a reinforcing bar, the less ability the bar has to control the width of the crack, resulting in wider cracks spaced further apart. Crack patterns at the peak load can be observed for all four specimens in Fig. 7.

Side cover spalling was observed for all four specimens. Based on the LVDT and LED target measurements, side cover spalling began at the flexural compression corners of the coupling beam as the stirrups began to yield, progressing towards midspan at the peak load, and showing visible spalling by the end of the test, as shown in Fig. 7. This side cover spalling phenomenon inherently causes localized changes in surface strains as the cover becomes delaminated from the core. This localized variation would directly affect the LED and LVDT measurements taken for Specimens CBF2, CBF3, and CBF4. CBF1 would see significantly less interference because the LVDTs were able to be mounted directly into the concrete core. Once the test was complete, all spalled cover was removed from the specimen as shown in Fig. 1(c) and Fig. 5 for Specimen CBF1 and Fig. 7 for all four specimens.

## ANALYTICAL PREDICTIONS

### Load-deformation response

The new version of the program Response was used to accurately predict the load-deformation response of the



Fig. 5—End of test for Specimen CBF1 with spalled cover removed.

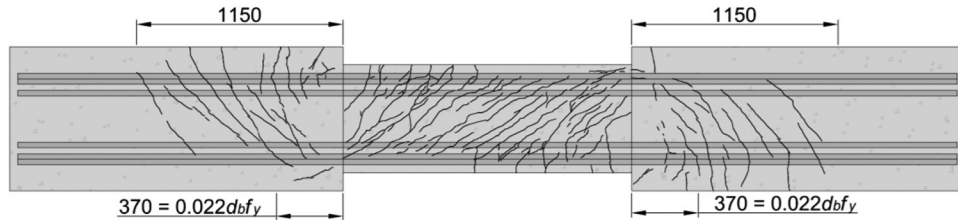


Fig. 6—Strain penetration length based on crack pattern for Specimen CBF1. (Note: Dimensions in mm; 1 mm = 0.0394 in.)

coupling beam specimens. These predictions are shown with the observed load-deformation response in Fig. 8. Also included in the figure are the predicted crack patterns and the deflected shape generated by the program. Predictions for Specimens CBF1, CBF2, and CBF3 were very accurate. The prediction for Specimen CBF4 was not as accurate in terms of the peak load; however, the predicted stiffness up to the predicted failure load accurately depicts the experimental data. The average test-to-predicted ratio for all four specimens was 1.04 for the shear strength and 1.14 for the tangential displacement at peak load. In Response, the effective length of the coupling beam was taken as the clear length of 1600 mm (63.0 in.) plus a distance of  $0.5d$  into the shear wall end blocks at each end, giving a total length of 2088 mm (82.3 in.). These extensions account for the localized deflections in the beam-wall joints and are recommended to be taken as approximately  $0.5h$ .<sup>12,19</sup> When the pattern of longitudinal reinforcement is known, as in this

case, the use of  $0.5d$  is more appropriate. To properly model the post-tensioning clamping force applied to the shear wall, the transverse reinforcement in the end blocks were prestressed in the model to a strain of  $1.1 \times 10^{-3}$  to create an equivalent concrete compressive stress of 2 MPa (290 psi). The concrete stress-strain relationship was modeled using the standard Popovics-Mander model<sup>20</sup> for confined concrete. The Vecchio-Collins 1986 model<sup>21</sup> for compression softening was also used.

### Shear stress-strain response

The program Membrane was used to predict the shear stress-strain response for specimen CBF1. The Membrane element was modeled using a longitudinal reinforcement ratio based on the effective shear depth of  $0.9d$ . The predicted stress-strain response is plotted in Fig. 9, along with the observed midspan shear strains measured by the LVDTs. Membrane predicted a failure shear stress of

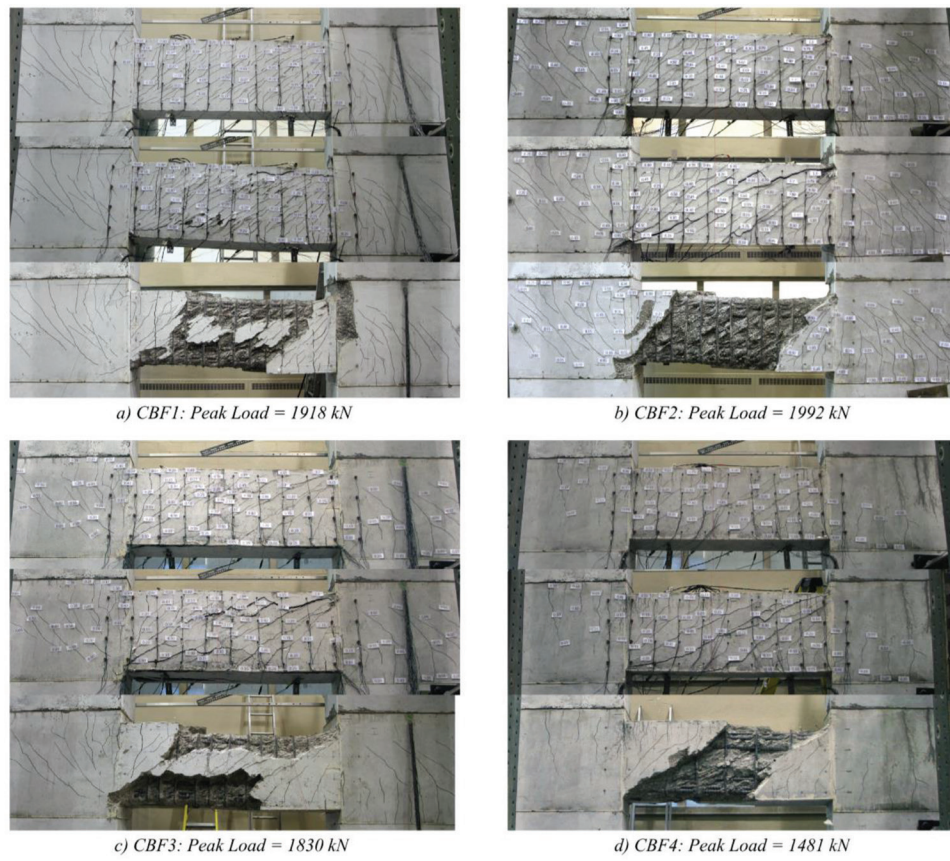


*Fig. 7—Coupling beam specimens at peak load, end of maximum deformation, and after spalled cover is removed. (Note: 1 kN = 0.225 kip.)*

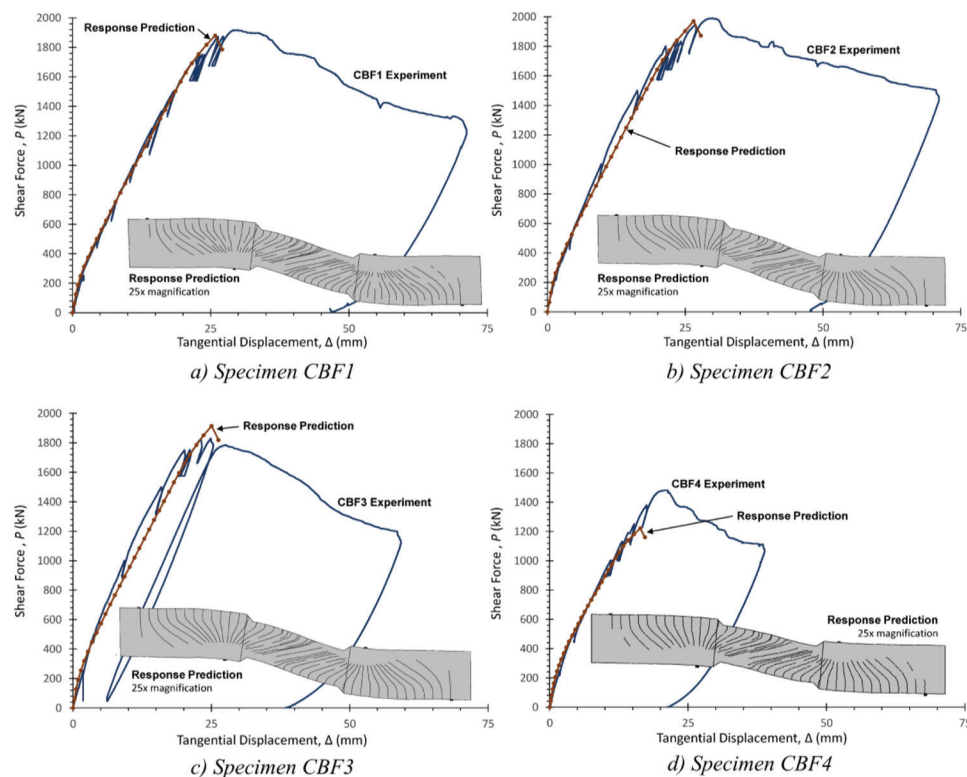


*Fig. 8—Comparison of observed and predicted load-deformation response generated by Response. (Note: 1 mm = 0.0394 in.; 1 kN = 0.225 kip.)*

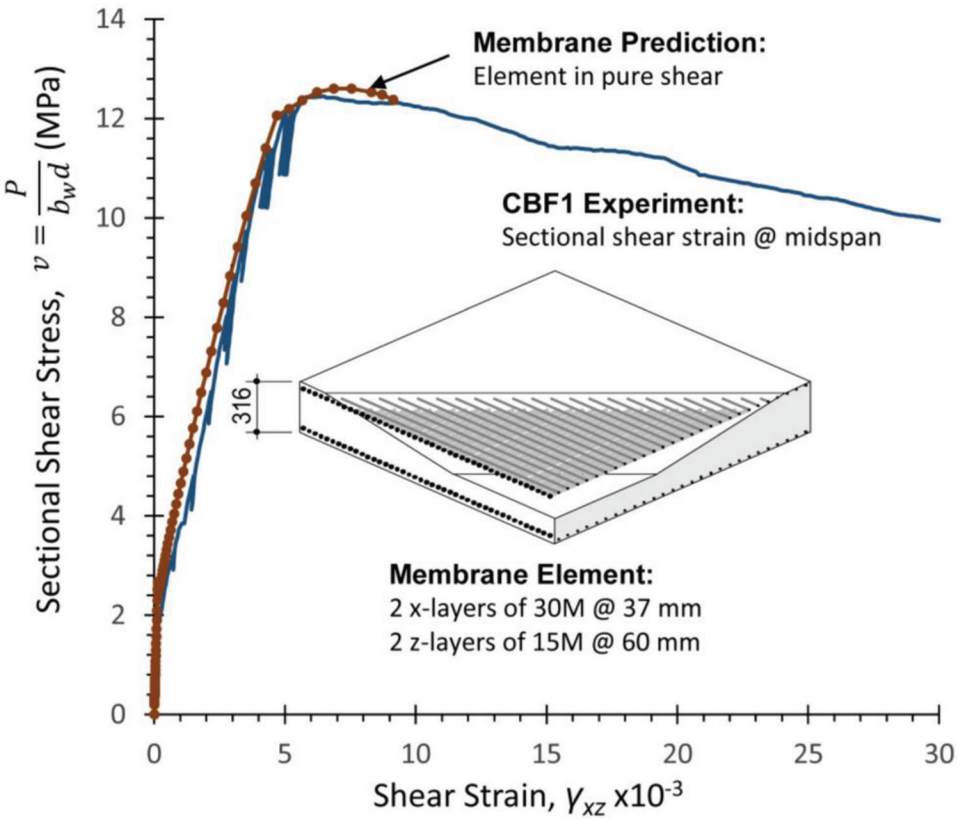


Fig. 9—Comparison of observed midspan shear strain for CBF1 and comparable membrane element loaded in pure shear generated by Membrane. (Note: 1 mm = 0.0394 in.; 1 MPa = 145 psi = 0.145 ksi.)

12.6 MPa (1830 psi) and corresponding shear strain of  $6.85 \times 10^{-3}$ , compared to an experimental peak shear stress of 12.4 MPa (1800 psi) and shear strain of  $6.50 \times 10^{-3}$ . These stresses and strains have test-to-predicted ratios of 1.02 and 1.05 respectively.

### Effective stiffness

An accurate coupling beam stiffness model must account for flexural and shear deformations, as well as local behavior in the beam-wall joints. Common linear models associated with these stiffness components are presented in Fig. 10 for specimen CBF1. The observed pre-peak load-deformation response of CBF1 is also included in Fig. 10 for comparison. The elastic flexural behavior for a coupling beam is commonly defined by the equation

$$\Delta = \frac{PL_e^3}{12E_c I_e} \quad (1)$$

where  $\Delta$  is the tangential displacement of the beam;  $P$  is the applied shear force;  $I_e$  is the effective moment of inertia; and  $L_e$  is the effective length, taken as 2088 mm (82.3 in.) to account for beam-wall joint behavior. The uncracked elastic analysis uses the transformed moment of inertia,<sup>12</sup>  $I_e = I_{trans}$ , of  $8450 \times 10^6$  mm<sup>4</sup> (20,580 in.<sup>4</sup>) due to the significant percentage of longitudinal reinforcement. At the stirrup yield load of 1696 kN (382 kip) for CBF1, the uncracked analysis predicts a displacement of 4.15 mm (0.17 in.). For the cracked elastic analysis, the ACI Code recommends

using  $I_e = 0.35I_g$ ; however, in this case, a value of  $0.35I_{trans}$  is used. This predicted cracked elastic response is shown in Fig. 10, having a predicted displacement of 11.9 mm (0.47 in.) at the stirrup yield load. This is only 53% of the measured beam deflection at stirrup yield. The linear model was able to accurately predict the beam stiffness up to a load of approximately 240 kN (54 kip), which was prior to the formation of shear cracks.

The effective shear modulus for diagonally cracked reinforced concrete coupling beams,  $G_{cr}$ , can be calculated using the equations<sup>22</sup>

$$G_{cr} = \frac{0.5E_c}{1 + \sqrt{\left(1 + \frac{1}{n\rho_l}\right)\left(1 + \frac{1}{n\rho_t}\right)}} \quad (2)$$

$$\Delta_{shear} = \frac{P}{b_w 0.9d} \cdot \frac{L_e}{G_{cr}} \quad (3)$$

where  $n$  is the modular ratio  $E_s/E_c$ ;  $\rho_l$  is the total longitudinal reinforcement ratio  $(A_s + A'_s)/b_w 0.9d$ ; and  $\rho_t$  is the transverse reinforcement ratio  $A_v/b_w s$ . The shear modulus for CBF1 is calculated to be 3088 MPa (448,000 psi). At the stirrup yield load of 1696 kN (382 kip), the displacement due to shear is predicted to be 8.26 mm (0.32 in.), which is 37% of the observed deflection. The cracked elastic flexural and shear contributions are combined in Fig. 10 to give a total displacement of 20.1 mm (0.79 in.) at stirrup yield, resulting in a test-to-prediction ratio of 1.11.

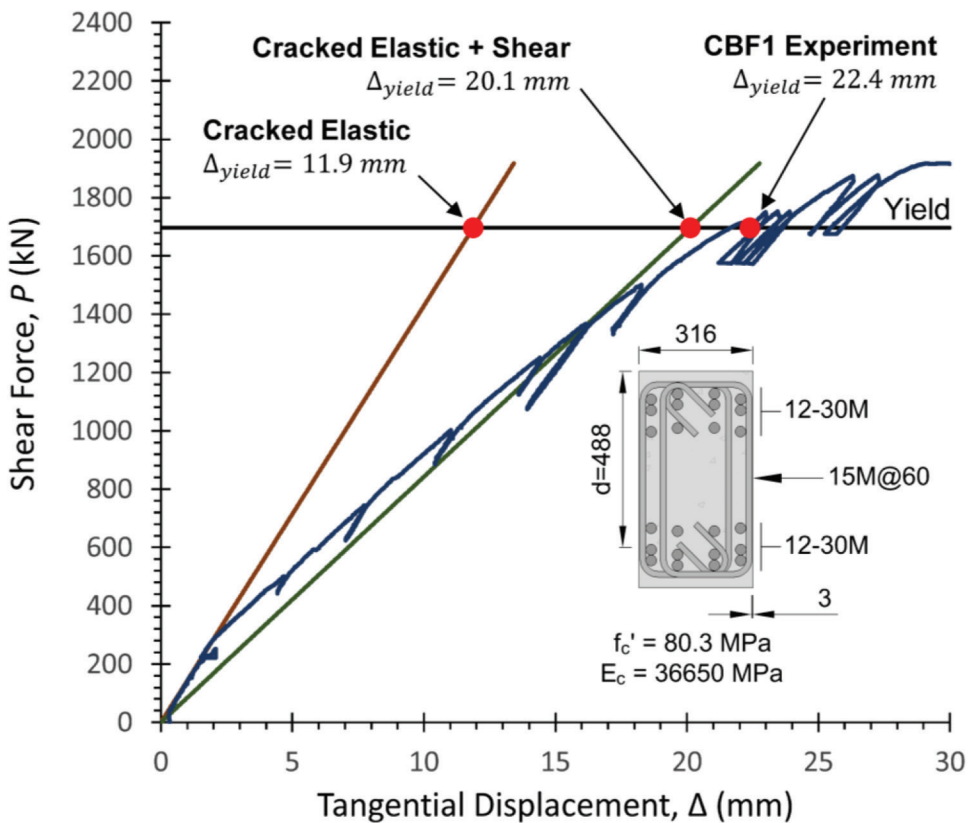


Fig. 10—Linear flexural and shear stiffness models compared to observed deformation for CBF1. (Note: 1 mm = 0.0394 in.; 1 kN = 0.225 kip.; 1 MPa = 145 psi = 0.145 ksi.)

### CODE PREDICTIONS OF SHEAR STRENGTH

The design requirements for coupling beams with conventional reinforcement layouts differ significantly between design codes. When designing these beams for shear, the ACI Code limits the steel contribution to shear capacity,  $V_s$ , to  $0.66\sqrt{f'_c b_w d}$  ( $8\sqrt{f'_c b_w d}$  in psi) to prevent an over-reinforced shear failure characterized by diagonal crushing of the concrete prior to yielding of the stirrups. The nominal shear capacity,  $V_n$ , is further limited to  $0.83\sqrt{f'_c b_w d}$  ( $10\sqrt{f'_c b_w d}$  in psi). Experiments<sup>23-25</sup> and analyses<sup>26</sup> have shown that these limits are very conservative for high-strength concrete beams with large amounts of shear reinforcement, with beam strengths in some cases double the ACI Code limit. Coupling beams with conventional reinforcement layouts are penalized by this limit and as a result may be unnecessarily deep. The CSA Code, based on the Modified Compression Field Theory,<sup>21</sup> permits higher percentages of shear reinforcement than the ACI Code by having an upper limit on shear capacity of  $0.22f'_c b_w d$ . This allows the beams to be shallower for the same shear strength. The CSA and ACI Code shear strength predictions for each of the four coupling beam specimens are presented in Table 2 along with the predictions made by program Response. The CSA code was able to accurately predict the ultimate shear capacity of the coupling beams with an average test-to-prediction ratio of 1.05 and a coefficient of variation of 8.5%. The predicted strengths calculated using the ACI code were less accurate, with an average test-to-prediction ratio of 1.45, the highest value being 1.67, and a coefficient of variation of 10.3%. These conservative predictions relate directly to the upper limits

Table 2—Comparison of observed and predicted peak shears

Specimen	Observed			Predicted		
	$f'_c$ , MPa	$\rho_z f_{yz}$ , MPa	$P_u$ , kN	$P_u$ , kN		
				Response	CSA	ACI
CBF1	80.3	8.9	1918	1880	1871	1147
CBF2	80.3	7.0	1992	1972	1907	1452
CBF3	66.5	7.0	1830	1915	1907	1321
CBF4	66.5	3.5	1481	1221	1213	1089
Average $P_{u-EXP}/P_{u-PRED}$				1.04	1.05	1.45
Coefficient of variation, %				8.6	8.5	10.3

Notes: 1 mm = 0.0394 in.; 1 kN = 0.225 kip; 1 MPa = 145 psi = 0.145 ksi.

on shear. It is recommended that these limits be liberalized to better accommodate heavily reinforced coupling beams.

### SIDE COVER SPALLING

This experimental program demonstrated that load-induced side cover spalling does occur for heavily reinforced coupling beams as they approach a shear failure. With the loss of this side cover, the effective width of the coupling beam,  $b_w$ , is reduced to the centerline of the outermost transverse reinforcement, and could potentially cause premature concrete crushing if not accounted for in the design.

Side cover spalling due to shear is caused by the change in direction of the diagonal compression stresses as they approach the corner of the member. The principal compression stress trajectory in the concrete side cover, shown

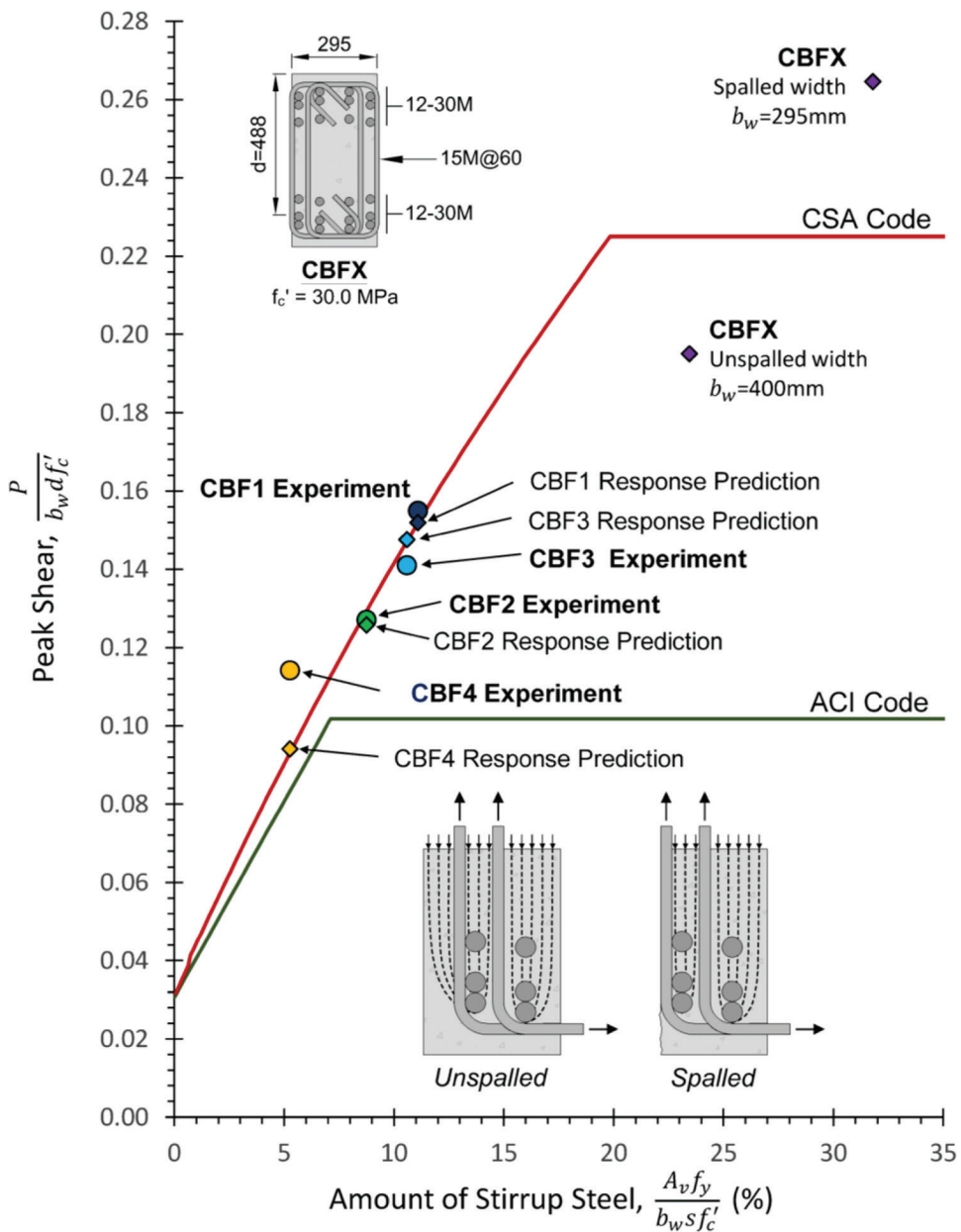


Fig. 11—Comparison of code predictions to observed failure loads, including influence of side cover spalling. (Note: 1 mm = 0.0394 in.; 1 kN = 0.225 kip.); 1 MPa = 145 psi = 0.145 ksi.)

in Fig. 11, curves in towards the corner longitudinal bar, resulting in principal tensile stresses that are perpendicular to the side face of the beam. At higher shear stresses, there can be enough perpendicular tension in the concrete side cover to cause it to split away from the reinforcement.

Side cover spalling had minimal impact on the observed shear strengths for the four coupling beam specimens of this project due to the unexpectedly high strengths of the concrete used. For these beams, yielding of the stirrups was predicted to govern failure whether the concrete cover was assumed to spall or not. Side cover spalling will significantly reduce the shear strength only if the loss of cover causes the remaining concrete core to crush in diagonal compression prior to yielding of the stirrups, or prior to the expected reduction in the angle of inclination of the diagonal compressive stresses in the concrete. To demonstrate this possibility of failure, coupling beam CBFX was assumed to have the same geometry

and reinforcement layout as CBF2 and CBF3 but with a 30 MPa (4350 psi) concrete strength. Because Response accurately predicted the failure shears for the four specimens, it was also used to predict the strength of CBFX with a spalled width of 295 mm (11.6 in.). This assumes the concrete cover spalls to the centerline of the outermost stirrups. Response predicted a peak load of 1142 kN (257 kip) with concrete crushing governing failure.

To compare this failure shear with the experimental and predicted values of CBF1 to CBF4, the shear strengths were normalized by the concrete strength and plotted with respect to the amount of shear reinforcement in Fig. 11. The CSA and ACI prediction curves are also included. From this figure, it can be seen that the ACI upper limit on shear capacity is less than half of the CSA upper limit on shear capacity, and that all of the experiments are significantly above the ACI limit. If cover spalling is accounted for and

a spalled width of 295 mm (11.6 in.) is used, the CSA code will somewhat under-predict the strength of CBFX, resulting in a safe design. However, if the unspalled width of 400 mm (15.8 in.) is used for CBFX, the CSA code over-predicts the shear strength, resulting in an unsafe coupling beam design. These data points are shown in Fig. 11. Accounting for the side cover spalling phenomenon is therefore important for heavily reinforced coupling beam designs that approach the concrete crushing limit.

## CONCLUDING REMARKS

The strength and stiffness of concrete coupling beams are important to the space efficiency and performance of high-rise concrete structures under lateral loads. This paper has described experiments that simulated coupling beam behavior to evaluate the shear strength provisions in design codes, show the power of Response in predicting the load-deflection behavior, and illustrate the importance of using a robust stiffness model. From these key aspects of the paper, the following conclusions have been drawn:

1. Shear-critical coupling beam designs, using well-detailed stirrups that exceed the ACI Code limits on shear capacity, can be a good solution for a coupled shear wall system that needs to resist high levels of shear with minimal beam depths. These beam designs are shown to not only be structurally sufficient, but have reasonable post-peak deformation capacity.

2. New program Response was able to accurately predict the load-deformation response of the four coupling beam specimens, with an average test-to-prediction ratio of 1.04 for the peak load and 1.14 for the associated displacement. Response is shown to be a powerful tool for predicting the behaviour of shear critical members.

3. To accurately model the stiffness of a coupled shear wall system, it is important to account for both flexural and shear deformations as well as beam-wall joint behavior. Ignoring any of these can result in an over-prediction of stiffness and under-prediction of lateral displacements.

4. Due to the very conservative upper limits on the steel contribution,  $V_s$ , and total strength,  $V_n$ , the ACI Code penalizes the predicted shear strength of heavily reinforced, high-strength concrete coupling beams. The average ACI test-to-prediction ratio was 1.45 for the four coupling beam specimens. It is recommended that these limits be liberalized to permit more efficient building designs.

5. The CSA Code was able to predict the peak loads with an average test-to-prediction ratio of 1.05. It is recommended that the CSA limit on shear capacity be used as a benchmark for developing new limits for the ACI Code.

6. Concrete side cover spalling can be a problem for heavily reinforced members with design strengths that approach the diagonal concrete crushing limit. The reduction in cross-sectional area can result in a premature concrete crushing failure. Results of this research indicate that concrete side cover spalling does occur for heavily reinforced, high-strength coupling beams, and therefore should be accounted for in the design process.

## AUTHOR BIOS

**Andrew W. Fisher** is a Structural EIT with Read Jones Christoffersen (RJC) Engineers, Toronto, ON, Canada. He received his bachelor's degree from the University of Waterloo, Waterloo, ON, Canada, in 2013 and his master's degree from the University of Toronto, Toronto, ON, Canada, in 2016.

**Evan C. Bentz**, FACI, is an Associate Professor of civil engineering at the University of Toronto. He received his bachelor's degree from the University of Waterloo in 1994 and his PhD from the University of Toronto in 2000. He is Chair of ACI Committee 365, Service Life Modeling, and is a member of Joint ACI-ASCE Committee 445, Shear and Torsion.

**ACI Honorary Member Michael P. Collins** is a University Professor in the Department of Civil Engineering at the University of Toronto. He received his bachelor's degree from the University of Canterbury, Christchurch, New Zealand, in 1964, and his PhD from the University of New South Wales, Sydney, NSW, Australia, in 1968. He is a member of Joint ACI-ASCE Committee 445, Shear and Torsion, and a past member of ACI Committee 318, Structural Concrete Building Code. His research interests include shear and torsion behavior and code provisions.

## ACKNOWLEDGMENTS

The authors would like to express their gratitude to the Natural Sciences and Engineering Research Council of Canada for a series of grants that have made possible the long-term research project on shear design of reinforced concrete at the University of Toronto.

## NOTATION

$A_b$	= area of reinforcing bar
$A_s$	= area of flexural tension reinforcement
$A'_s$	= area of flexural compression reinforcement
$A_v$	= area of shear reinforcement
$a_g$	= maximum aggregate size
$b_w$	= web width
$d$	= effective depth
$d_b$	= bar diameter
$d_y$	= shear depth = 0.9d
$E_c$	= modulus of elasticity of concrete
$E_s$	= modulus of elasticity of steel
$f'_c$	= concrete strength measured on test day
$f_u$	= measured ultimate strength of reinforcement
$f_y$	= measured yield strength of reinforcement
$f_{yz}$	= measured yield strength of z-direction/transverse reinforcement
$G_{cr}$	= shear modulus for diagonally cracked reinforced concrete
$h$	= overall member height
$I_e$	= effective moment of inertia
$I_g$	= gross moment of inertia
$I_{trans}$	= transformed moment of inertia
$L$	= clear length
$L_e$	= effective length
$l_{yp}$	= yield penetration length
$M$	= applied moment
$n$	= modular ratio = $E_s/E_c$
$P$	= applied shear force
$P_u$	= ultimate applied shear force
$P_{u-EXP}$	= experimental ultimate applied shear force
$P_{u-PRED}$	= predicted ultimate applied shear force
$s$	= stirrup spacing
$V$	= shear force
$V_n$	= nominal shear strength
$V_s$	= shear strength provided by shear reinforcement
$\nu$	= sectional shear stress
$W_{self}$	= self-weight
$\Delta$	= tangential displacement
$\Delta_{yield}$	= tangential displacement at first stirrup yield
$\Delta_{shear}$	= tangential displacement due to shear
$\varepsilon_{sh}$	= steel strain at strain hardening
$\varepsilon_{xx}$	= x-direction/longitudinal reinforcement strain
$\varepsilon_{zz}$	= z-direction/transverse reinforcement strain
$\varepsilon_u$	= steel strain at ultimate strength
$\varepsilon_z$	= average vertical strain over web height
$\gamma_{xz}$	= shear strain
$\rho_l$	= total percentage of longitudinal reinforcement
$\rho_t$	= percentage of transverse reinforcement
$\rho_z$	= percentage of z-direction/transverse reinforcement
$\sigma$	= post-tensioning bar stress

## REFERENCES

1. Paulay, T., "Coupling Beams of Reinforced Concrete Shear Walls," *Journal of the Structural Division*, ASCE, V. 97, No. 3, Mar. 1971, pp. 843-862.
2. Paulay, T., and Binney, J. R., "Diagonally Reinforced Coupling Beams of Shear Walls," *Shear in Reinforced Concrete*, SP-42, American Concrete Institute, Farmington Hills, MI, 1974, pp. 579-598.
3. Barney, G. B.; Shiu, K. N.; Rabbit, B. G.; Fiorato, A. E.; Russell, H. G.; and Corley, W. G., *Behaviour of Coupling Beams under Load Reversals*, Portland Cement Association, Skokie, IL, 1980.
4. Tassios, T. P.; Moretti, M.; and Bezias, A., "On the Behaviour and Ductility of Reinforced Concrete Coupling Beams of Shear Walls," *ACI Structural Journal*, V. 93, No. 6, Nov.-Dec. 1996, pp. 711-720.
5. Xiao, Y.; Esmaeily-Ghasemabadi, A.; and Wu, H., "High-Strength Concrete Short Beams Subjected to Cyclic Shear," *ACI Structural Journal*, V. 87, No. 1, May-June 1999, pp. 392-399.
6. Galano, L., and Vignoli, A., "Seismic Behaviour of Short Coupling Beams with Different Reinforcement Layouts," *ACI Structural Journal*, V. 97, No. 6, Nov.-Dec. 2000, pp. 876-885.
7. Kwan, A. K. H., and Zhao, Z. Z., "Cyclic Behaviour of Deep Reinforced Concrete Coupling Beams," *Structures and Buildings*, V. 152, No. 3, Aug. 2002, pp. 283-293.
8. Naish, D.; Fry, J. A.; Klemencic, R.; and Wallace, J. W., "Reinforced Concrete Coupling Beams—Part I: Testing," *ACI Structural Journal*, V. 110, No. 6, Nov.-Dec. 2013, pp. 1057-1066.
9. Lim, E.; Hwang, S.-J.; Cheng, C.-H.; and Lin, P.-Y., "Cyclic Tests of Reinforced Concrete Coupling Beam with Intermediate Span-Depth Ratio," *ACI Structural Journal*, V. 113, No. 3, May-June 2016, pp. 515-524.
10. ACI Committee 318, "Building Code Requirements for Structural Concrete (ACI 318-14) and Commentary (ACI 318R-14)," American Concrete Institute, Farmington Hills, MI, 2014, 520 pp.
11. PEER/ATC 72-1, "Modeling and Acceptance Criteria for Seismic Design and Analysis of Tall Buildings," Applied Technology Council, Redwood City, CA, and Pacific Earthquake Engineering Research Center, University of California, Berkeley, Berkeley, CA, Oct. 2010, 226 pp.
12. Wight, J. K., and MacGregor, J. G., *Reinforced Concrete—Mechanics and Design*, sixth edition, Prentice Hall, Upper Saddle River, NJ, 2012, 1157 pp.
13. Naish, D.; Fry, J. A.; Klemencic, R.; and Wallace, J. W., "Reinforced Concrete Coupling Beams—Part II: Modeling," *ACI Structural Journal*, V. 110, No. 6, Nov.-Dec. 2013, pp. 1067-1076.
14. CSA A23.3-14, "Design of Concrete Structures," Canadian Standards Association, Mississauga, ON, Canada, 2014, 297 pp.
15. Bentz, E. C., "Response," <http://www.ecf.utoronto.ca/~bentz/r2k.htm>. (last accessed Aug. 23, 2017)
16. Bentz, E. C., "Membrane," <http://www.ecf.utoronto.ca/~bentz/m2k.htm>. (last accessed Aug. 23, 2017)
17. Fisher, A. W., "Shear Performance of Heavily Reinforced High-Strength Concrete Coupling Beams," master's thesis, University of Toronto, Toronto, ON, Canada, June 2016, 246 pp.
18. Paulay, T., and Priestley, M. J. N., *Seismic Design of Reinforced Concrete and Masonry Buildings*, John Wiley & Sons, Inc., New York, 1992, 744 pp.
19. Schwaighofer, J., and Collins, M. P., "An Experimental Study of the Behaviour of Reinforced Concrete Coupling Slabs," *ACI Journal Proceedings*, V. 74, No. 3, Mar. 1977, pp. 123-127.
20. Mander, J.; Priestley, M.; and Park, R., "Theoretical Stress-Strain Model for Confined Concrete," *Journal of Structural Engineering*, ASCE, V. 114, No. 8, Sept. 1988, pp. 1804-1826.
21. Vecchio, F. J., and Collins, M. P., "The Modified Compression Field Theory for Reinforced Concrete Elements Subjected to Shear," *ACI Journal Proceedings*, V. 83, No. 2, Mar.-Apr. 1986, pp. 219-231.
22. Collins, M. P., "Towards a Rational Theory for RC Members in Shear," *Journal of the Structural Division*, ASCE, V. 104, No. 4, Apr. 1978, pp. 649-666.
23. Lee, J.-Y., and Hwang, H.-B., "Maximum Shear Reinforcement of Reinforced Concrete Beams," *ACI Structural Journal*, V. 107, No. 5, Sept.-Oct. 2010, pp. 580-588.
24. Reineck, K.-H.; Bentz, E.; Fitik, B.; Kuchma, D. A.; and Bayrak, O., "ACI-DAFSib Databases for Shear Tests on Slender Reinforced Concrete Beams with Stirrups," *ACI Structural Journal*, V. 111, No. 5, Sept.-Oct. 2014, pp. 1147-1156.
25. Proestos, G. T.; Bae, G.-W.; Cho, J.-Y.; Bentz, E. C.; and Collins, M. P., "Influence of High-Strength Reinforcing Bars on Shear Response of Containment Walls," *ACI Structural Journal*, V. 113, No. 5, Sept.-Oct. 2016, pp. 917-928.
26. Lee, J. L.; Kuchma, D. A.; Baker, W.; and Novak, L. C., "Design and Analysis of Heavily Loaded Reinforced Concrete Link Beams for Burj Dubai," *ACI Structural Journal*, V. 105, No. 4, July-Aug. 2008, pp. 451-459.